analytical chemistry

Letter

pubs.acs.org/ac

Serially Ordered Magnetization of Nanoclusters via Control of Various Transition Metal Dopants for the Multifractionation of Cells in Microfluidic Magnetophoresis Devices

Byunghoon Kang,[†] Bumjoon Cha,[†] Bongsoo Kim,[‡] Seungmin Han,[†] Moo-Kwang Shin,[†] Eunji Jang,[†] Hyun-Ouk Kim,[†] Seo Ryung Bae,[†] Unyong Jeong,[∥] Il Moon,[†] Hye yeong Son,[§] Yong-Min Huh,*[,§] and Seungjoo Haam*[,†]

[†]Department of Chemical and Biomolecular Engineering, Yonsei University, Seoul 120-749, South Korea

[‡]Department of Materials Science and Engineering, Yonsei University, Seoul 120-749, South Korea

[§]Department of Radiology and Research Institute of Radiological Science, College of Medicine, Yonsei University, Seoul 120-752, South Korea

[∥]Department of Materials Science and Engineering, Pohang University of Science and Technology, 77 Cheongam-Ro, Nam-gu, Pohang 120-784, Korea

Supporting Information

ABSTRACT: A novel method (i.e., continuous magnetic cell separation in a microfluidic channel) is demonstrated to be capable of inducing multifractionation of mixed cell suspensions into multiple outlet fractions. Here, multicomponent cell separation is performed with three different distinguishable magnetic nanoclusters ($MnFe_2O_4$, Fe_3O_4, and $CoFe_2O_4$), which are tagged on A431 cells. Because of their mass magnetizations, which can be ideally altered by doping with magnetic atom compositions (Mn, Fe, and Co), the trajectories of cells with each magnetic nanocluster in a flow are shown to be distinct when dragged under the same external magnetic field; the rest of the magnetic characteristics of the nanoclusters are identically fixed. This proof of concept study, which utilizes the magnetization-controlled nanoclusters (NCs), suggests that precise and effective multifractionation is achievable with high-throughput and systematic accuracy for dynamic cell separation.

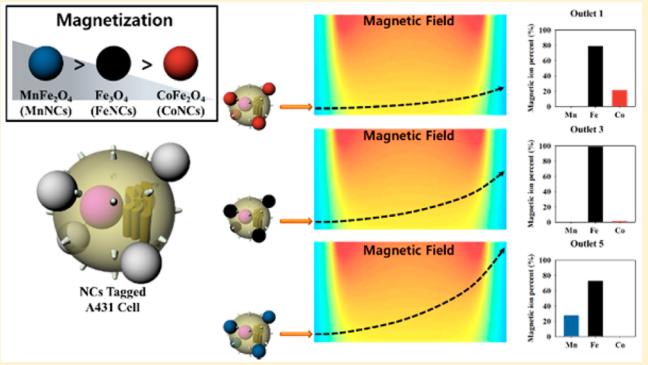

Extraction of homogeneous cell types from heterogeneously distributed cell populations is essential throughout experimental biology and medicine (e.g., drug delivery, stem cell therapy, regenerative medicine, cancer therapy, and HIV pathogenesis).[1−7] Therefore, efficient and facile separation techniques are greatly preferred in order to provide methods with high purity, high yield, and consistent cell functions. One of the most common and widely used cell separation techniques is fluorescence-activated cell sorting (FACS), which is based upon the specific light scattering and fluorescent characteristics of each cell.[8] FACS can sort heterogeneous mixtures of biological cells, even those with similar densities, into two or more containers; this is done one cell at a time.[8] However, FACS faces several constraints such as the high cost of its instrumentation and operation, potentially long analysis times, the risk of cell damage at high flow rates, and the requirement of a pretreatment with fluorescent markers.[8] Thus, a more facile alternative (i.e., immunomagnetic cell separation) was developed. In this technique, cells are labeled with magnetic beads and separated from the bulk of the sample using magnetic forces. Magnetic-activated cell sorting (MACS) has received much attention because of its rapid separation speed, low cost, high purity outputs, and lower degree of damage to the cells.[9,10] However, for the magnetic beads synthesized via conventional coprecipitation methods in MACS, it is difficult to maintain uniform magnetism, crystallinity, and size.[11,12] Hence, synthesized magnetic beads may possess both ferro- and super para-magnetism, which can demand the use of additional purification steps.[11] Furthermore, because current separation techniques rely only on the existence of magnetic tagging moieties, bimodal isolation is not yet possible. Therefore, efficient multifractionation to sort diverse types of cell populations, while simultaneously obtaining high-throughput, is highly recommended in order to minimize both the separation time and the associated cost per assay relative to conventional magnetic separation.[7,13−21] For the simultaneous separation of various cell populations, we

Received: October 29, 2015
Accepted: December 31, 2015
Published: December 31, 2015

DOI: 10.1021/acs.analchem.5b04111
Anal. Chem. 2016, 88, 1078−1082

first investigated the mobility of cells tagged with magnetic nanoclusters doped with various transition metals; these cells exhibit distinct differences in their magnetic intensities. Herein, multifractionating cell separation is demonstrated by utilizing three different types of magnetic nanoclusters composed of different grains (MFe_2O_4, M = Mn, Fe, and Co), which exhibit differentiated mass magnetization value but identical cluster sizes.[22−24] Next, these magnetic nanoclusters (MnNC, FeNC, and CoNC) were tagged onto the human epidermoid carcinoma cell line (A431, ATCC CRL-1555) to verify their multifractionated cell sorting capabilities by utilizing their distinct magnetizations.[25] Consequently, the differences in the cell mobility that resulted from the differentiated magnetic magnetization leads to effective multiseparation in the module of a fluidic channel (Figure S3). Furthermore, to confirm that the separation results coincide with theoretical modeling, we calculated the Lagrangian trajectories of cells treated with the three different types of magnetic nanoclusters (see Scheme 1).

Scheme 1. Schematic Representation of Component Control of Magnetic Nanoclusters, Trajectory Study for Cell Multifractionation

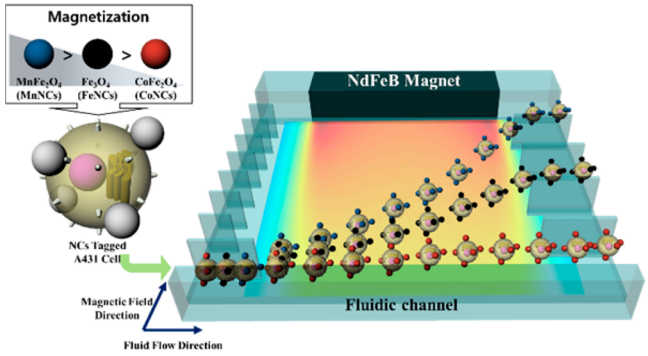

The synthesis of a series of transition metal-doped magnetic nanoclusters (MnNC, FeNC, and CoNC) was first initialized by reducing iron chloride, manganese chloride, and cobalt chloride, respectively. Magnetic nanoclusters were then prepared via one-pot synthesis of an altered solvothermal reaction[24] at 220 °C with poly(acrylic acid) (PAA) as an electrostatic stabilizer; PAA is used because the carboxylate functional group (COO−) of PAA possesses a robust coordination affinity to transition metals,[23] which enables antibody (CETUXIMAB, Erbitux) conjugation. In order to ascertain that the magnetization of the three synthesized types of magnetic nanoclusters (which differ only in their composition), the other variables that can affect the magnetization (e.g., cluster size and surface modification) were identically maintained.

First, the grain crystallinity and diameter of each magnetic nanocluster were analyzed. X-ray diffraction (XRD, Ultima3 X-ray diffractometer, Rigaku) patterns indicated that the crystallinity peaks were identical within the series of magnetic nanoclusters (MnNC (JCPDS 74-2403), FeNC (JCPDS 75-1609), and CoNC (JCPDS 22-1068); Figure S1a in the Supporting Information). Additionally, from the XRD patterns, the grain diameters of the magnetic nanoclusters were calculated using the Debye−Scherrer equation. The average grain diameters of MnNC, FeNC, and CoNC were 5.8, 5.9, and 6.0 nm, respectively, indicating that similar grain crystallinities and diameters were well maintained.[26] Next, the amount of the PAA layer was estimated by using thermogravimetric analysis (TGA, SDT-Q600, TA Instruments); this showed values of 87%, 85%, and 84% for MnNC, FeNC, and CoNC, respectively (Figure S1b). The magnetization of magnetic nanoclusters depends on the degree of grain packing in a single cluster,[27,28] which can be represented as the organic−inorganic ratio. Therefore, to maintain uniform magnetization, the organic−inorganic ratio is also a crucial factor to consider during the welding process to form nanoclusters. Scanning electron microscopy (SEM, JEOL JSM-6701F) showed that the synthesized MnNC, FeNC, and CoNC (Figures 1a−c) were

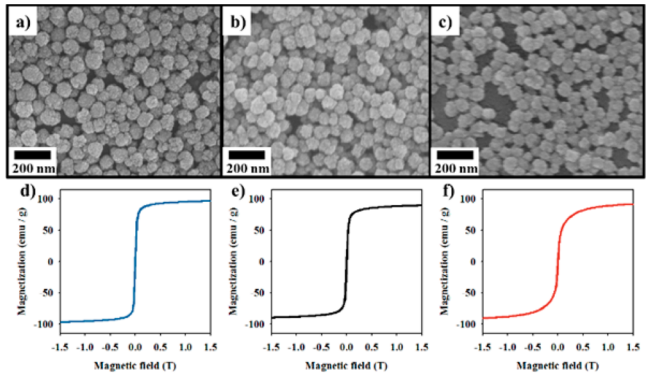

Figure 1. SEM images of different compositions (a) MnNCs, (b) FeNCs, (c) CoNCs and their magnetic hysteresis loops of (d) MnNCs, (e) FeNCs, and (f) CoNCs.

monodisperse in size. Their diameters, obtained via laser scattering (ELS-Z, Otsuka Electronics), were 108.5 ± 8.9 nm, 106.9 ± 8.9 nm, and 102.2 ± 9.0 nm, respectively (Figure S1c). In addition, the negative charges of these nanoclusters (measured from the zeta-potential, ELS-Z, Otsuka Electronics) were attributed to the presence of carboxylic groups (PAA) (Figure S1d), which are essential for conjugation with the antibodies of cells during the formation of amide bonds. Consequently, for the synthesis of magnetic nanoclusters, all other variables (except for the compositions) were consistently maintained to control the magnetization.

The synthesized magnetic nanoclusters maintained a combined spinel structure that is dissimilar to most metal ferrites, which typically exhibit an inverse spinel structure. When an external magnetic field was applied to this spinel structure, the magnetic spins in O_h (octahedral sites are occupied by M^{2+} and Fe^{3+}) aligned parallel to the direction of the external magnetic field; however, those in T_d (tetrahedral sites are occupied by Fe^{3+}) aligned antiparallel to the magnetic field.[25] Therefore, $MnFe_2O_4$ (manganese atom has five unpaired d orbital electrons) theoretically exhibited the highest magnetization of 15 emu per gram. The magnetization declined as M^{2+} changed from Fe^{2+} to Co^{2+}, causing the magnetic spin magnitude to decrease from approximately 12 to 9 emu per gram. Figure 1d−f shows the magnetization curves of nanoclusters at room temperature obtained from a vibrating sample magnetometer (VSM, model-7407, Lakeshore). The density of the generated magnetic flux was approximately 2000*g*, and the resulting mass magnetization values were 88.32, 80.74, and 68.31 emu per gram for MnNCs, FeNCs, and CoNCs, respectively. Furthermore, these differences in the mass magnetization value of nanoclusters (according to the change in composition) will become proportionally more distinct as their volumes are increased. Likewise, the results of

DOI: 10.1021/acs.analchem.5b04111
Anal. Chem. 2016, 88, 1078−1082

the theoretical calculations and VSM verify the feasibility of multifractionation using nanoclusters with modified compositions. First, A431 cells were treated with the as-synthesized nanoclusters to determine the appropriate particle concentration for cell surface attachment prior to in vitro experiments. In addition, the cytotoxicity of these nanoclusters against A431 cells was verified using the MTT assay (Figure S2, cell proliferation kit (Roche)); this showed that a treatment of less than 1 μg of nanoclusters exhibited reliable viability where 80% of the cells survived. To label the cells with NCs, equal concentrations of antibodies were attached to the particles beforehand. Next, A431 cells were incubated for a short period of time (0.5 h) with antibody-tagged NCs to induce adherence of the particles to the cell surface. To identify the nanoclusters that are affixed to the cell surface (not internalized), nanocluster-labeled A431 cells were fixed and cut in parallel sections for TEM imaging (Figure 2a–c, JEM-2100F, JEOL

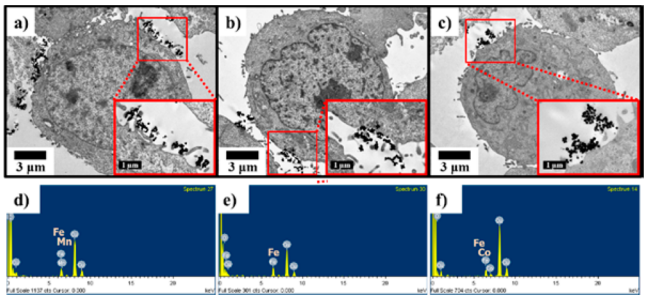

Figure 2. Cross-sectional TEM image (a,b,c), EDX analysis (d,e,f) of A431 cells incubated with (a,d) MnNCs, (b,e) FeNCs, and (c,f) CoNCs.

Ltd.). TEM images confirmed that small agglomerates of NCs were distributed on the extracellular surface, demonstrating that nanoclusters were successfully affixed onto the cell surface. Furthermore, the compositions of NCs adhered onto the surface of the cells were confirmed by TEM and EDX (energy-dispersive X-ray spectroscopy; Figure 2d–f). The approximate number of attached nanoclusters was calculated via inductively coupled plasma optical emission spectrometry (ICP-OES, Thermoelectron corporation, USA).

The principle of continuous flow magnetic separation implies that magnetic objects are deflected from the sample flow stream by the application of a magnetic field that is perpendicular to the direction of flow. The magnetophoresis chip design features an inlet channel for the cell suspension (200 μm wide), a branched inlet network for the buffer solution, a 25 mm long and 2.6 mm wide separation chamber (supported by 10 square posts), as well as 10 outlet channels (200 μm wide) that merge into five separate outlets. The buffer flows for each inlet, including the cell inlet, were controlled to have equal volumetric flow rates in order to minimize the velocity distribution in the microfluidic channel; thus, the flow was assumed to behave as a plug flow. A permanent magnet was placed next to the channel to obtain the maximum magnetic force on the labeled cells. The magnetic field was generated by an NdFeB magnet that was 40 mm long, 25 mm wide, and 25 mm thick. (Figure S3). The magnetic field was 0.26 T at the magnet surface and 0.20 T in the middle of the separation chamber. During multifractionation, the introduced labeled cells were deflected onto the magnet due to the external magnetic force. This deflection behavior gradually increased as the magnetic force against the NCs increased when the labeled cells approached the magnet. The resulting trajectories are shown as curved tracks in Figure 3 and video clip (video

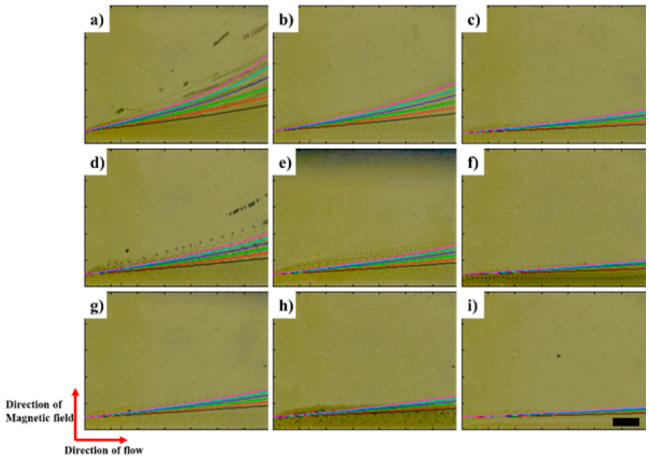

Figure 3. Trajectory and simulation images of cells' mobility labeled MnNCs (a,d,g), FeNCs (b,e,h), and CoNCs (c,f,i) at each total flow late 90 μL min^{-1} (a,b,c), 135 μL min^{-1}(d,e,f), and 180 μL min^{-1}(g,h,i). (Scalebar: 500 μm).

S1–S9). The deflection behaviors of the labeled cells were also supported by the theoretically calculated cell tracking results. Force balance equations for the magnetic force and the drag force on the labeled cell were applied to the theoretical simulation; other minor forces were neglected (more details are included in the Supporting Information). The deflection of each flow was expressed as the angle between the incline of the early profile and the bottom of the channel (x-axis). Cells tagged with NCs were transported in the channel by the net force of fluid motion and other forces directed by the magnetic field. The plotting equation for the trajectory of the cell mobility is defined in eq 1:

$$\theta = c(e^{aX} - 1) \quad (1)$$

Here, the x-axis is the direction of the fluid, the y-axis is the direction of the magnetic fluid, and θ is the angle between the tangent to the trajectory and the x-axis (Figure S4). It can be assumed that the velocity toward the x-axis of the NC-tagged-cells is the same as the fluid velocity because the fluid behavior is assumed to be that of an ideal plug flow; all of the fluid velocities along the x-axis at every position along the y-axis are the same. The velocity along the y-axis (Vy) of moving cells under the influence of the magnetic field was affected by the cell's mobility. The magnetization value difference between the various transition metals doped onto NCs-tagged cells can cause the cells to have different magnetic mobilities. This variance resulted in cells with different Vy, such that MnNC-cells were the fastest and CoNC-cells were the slowest (among the cells doped with Mn-, Fe-, and CoNCs). A larger solution for eq 1 indicates that the effect of the magnetic field on the cell mobility was significant and also that the cells' magnetic mobility is sufficiently large such that we can compare the properties of each NC. The "a" values of each component are shown in Table 1.

A faster flow rate leads to higher throughput; however, when this happens, the exposure time under the magnetic field is shortened. This results in a smaller degree of deflection, which leads to less effective separation. Considering the flow velocity

DOI: 10.1021/acs.analchem.5b04111
Anal. Chem. 2016, 88, 1078–1082

Table 1. Constant "*a*"

(Unit : mm^{-1})

	MnNCs tagging cell	FeNCs tagging cell	CoNCs tagging cell
90 μℓ/min	0.4105 ± 0.1673	0.2360 ± 0.0987	0.1051 ± 0.0343
135 μℓ/min	0.2012 ± 0.0857	0.1217 ± 0.0598	0.0538 ± 0.0199
180 μℓ/min	0.1168 ± 0.0671	0.0675 ± 0.0447	0.0221 ± 0.0225

results, microfluidic magnetophoresis was demonstrated at a flow rate of 135 μL min^{-1} with FeNCs-, MnNCs-, and CoNCs-labeled A431 cells flowing into the outlet syringes. These results were analyzed using ICP-OES. CoNCs-labeled cells were found to leave the critical section through outlets 1 and 2, FeNCs-treated cells were collected into outlets 3 and 4, and cells with MnNCs mostly left via outlet 5 (Figure S6). For labeled cells at a flow rate of 90 μL min^{-1}, MnNC-labeled cells left via outlet 5; however, they were also found to be adhered onto the inner walls heading toward outlet 5. FeNC-tagged cells were mostly observed at the outlets 3 and 4, whereas CoNCs-tagged cells were found throughout outlets 2 and 3, leading to unspecific separation. (Figure S5) When the flow rate was raised to 180 μL min^{-1}, the influence of the flow on the cells is much stronger than the influence of the magnetic field. Therefore, sorting is inaccurate and a combination of cells are evacuated via outlets 1, 2, and 3 (Figure S7). The deflection path (i.e., the outlet taken by a cell) is influenced by both the flow rate and the NCs load. A slower flow rate and higher magnetization loading resulted in a larger degree of deflection, causing the cells to be deposited at a higher outlet number.

Consequently, magnetic cell separation in a microfluidic system containing five outlets was successfully performed. Cells were deflected and carried out into different outlet channels depending on their magnetic content. The successful demonstration of the separation of A431 cells was based on the separation of cells with different magnetization. This method allows for high-throughput and cell preservation, successfully overcoming the current shortcomings of FACS and MACS.

A multifractionation method for magnetic cell separation (as a function of the mass magnetization of NCs) has been presented and evaluated using an A431 cell model. Three types of metal components (Mn, Fe, and Co) with distinct magnetization differences were chosen and doped into magnetic nanoclusters to form MnNC, FeNC, and CoNC, respectively. The magnetization of each NC was as expected; MnNCs revealed the strongest response, followed by FeNCs and CoNCs, showing remarkable potential for multifractionation of the target cells. The sorting performance was applied to in vitro studies with A431 cells and demonstrated excellent sorting efficiencies. These results agree with those obtained from simulations. This system demonstrates the ability to separate various kinds of homogeneous and heterogeneous cells by taking advantage of a range of magnetizations.

■ ASSOCIATED CONTENT

Supporting Information

The Supporting Information is available free of charge on the ACS Publications website at DOI: 10.1021/acs.analchem.5b04111.

Video clips (ZIP)

Additional material analysis data, system setup, and experimental method (PDF)

■ AUTHOR INFORMATION

Corresponding Authors

*Phone: +82-2-2123-2751. Fax: +82-2-312-6401. E-mail: haam@yonsei.ac.kr.

*E-mail: ymhuh@yuhs.ac.

Author Contributions

B. Kang, Y.-M. Huh, and S. Haam were involved in all stages of design of experiments and interpretation of the results. B. Cha and I. Moon carried out simulation of trajectories about NCs-tagged cells in a microfluidic channel. B. Kim and U. Jeong carried out fabrication of the microfluidic channel. B. Kang, S. Han, M.-K. Shin, E. Jang, H.-O. Kim, S.R. Bae, and H.Y. Son carried out data collection and helped to write the paper.

Notes

The authors declare no competing financial interest.

■ ACKNOWLEDGMENTS

This research was supported by the Bio & Medical Technology Development Program of the National Research Foundation (NRF) funded by the Korean government (MEST) (Grant 2012050077).

■ REFERENCES

(1) Armstrong, A. J.; Marengo, M. S.; Oltean, S.; Kemeny, G.; Bitting, R. L.; Turnbull, J. D.; Herold, C. I.; Marcom, P. K.; George, D. J.; Garcia-Blanco, M. A. *Mol. Cancer Res.* **2011**, *9*, 997−1007.

(2) Chen, Y.; Li, P.; Huang, P. H.; Xie, Y.; Mai, J. D.; Wang, L.; Nguyen, N. T.; Huang, T. J. *Lab Chip* **2014**, *14*, 626−645.

(3) Chin, L.; Andersen, J. N.; Futreal, P. A. *Nat. Med.* **2011**, *17*, 297−303.

(4) Tomlinson, M. J.; Tomlinson, S.; Yang, X. B.; Kirkham, J. *J. Tissue Eng.* **2013**, *4*, 2041731412472690.

(5) Wognum, A. W.; Eaves, A. C.; Thomas, T. E. *Arch. Med. Res.* **2003**, *34*, 461−475.

(6) Zborowski, M. Chalmers, J. J.. *Magnetic Cell Separation*, 1st ed.; Elsevier: Amsterdam, The Netherlands, 2008.

(7) Shields, C. W., IV; Reyes, C. D.; Lopez, G. P. *Lab Chip* **2015**, *15*, 1230−1249.

(8) Robinson, J. P. In *Encyclopedia of Biomaterials and Biomedical Engineering*; Wnek, G. E., Bowlin, G. L., Eds.; Marcel Dekker, Inc.: New York, 2004; pp 630−640.

(9) Thiel, A.; Scheffold, A.; Radbruch, A. *Immunotechnology* **1998**, *4*, 89−96.

(10) Miltenyi, S.; Muller, W.; Weichel, W.; Radbruch, A. *Cytometry* **1990**, *11*, 231−238.

(11) Grutzkau, A.; Radbruch, A. *Cytometry, Part A* **2010**, *77*, 643−647.

(12) Kandpal, N. D.; Sah, N.; Loshali, R.; Joshi, R.; Prasad, J. *J. Sci. Indus. Res.* **2014**, *73*, 87−90.

(13) Pamme, N.; Eijkel, J. C. T.; Manz, A. *J. Magn. Magn. Mater.* **2006**, *307*, 237−244.

(14) Pamme, N.; Wilhelm, C. *Lab Chip* **2006**, *6*, 974−980.

(15) Robert, D.; Pamme, N.; Conjeaud, H.; Gazeau, F.; Iles, A.; Wilhelm, C. *Lab Chip* **2011**, *11*, 1902−1910.

(16) Schneider, T.; Moore, L. R.; Jing, Y.; Haam, S.; Williams, P. S.; Fleischman, A. J.; Roy, S.; Chalmers, J. J.; Zborowski, M. *J. Biochem. Biophys. Methods* **2006**, *68*, 1−21.

(17) Xu, J.; Mahajan, K.; Xue, W.; Winter, J. O.; Zborowski, M.; Chalmers, J. J. *J. Magn. Magn. Mater.* **2012**, *324*, 4189−4199.

(18) Adams, J. D.; Kim, U.; Soh, H. T. *Proc. Natl. Acad. Sci. U. S. A.* **2008**, *105*, 18165−18170.

(19) Jin, X.; Chalmers, J. J.; Zborowski, M. *Anal. Chem.* **2012**, *84*, 4520−4526.

(20) Moore, L. R.; Williams, P. S.; Nehl, F.; Abe, K.; Chalmers, J. J.; Zborowski, M. *Anal. Bioanal. Chem.* **2014**, *406*, 1661−1670.

DOI: 10.1021/acs.analchem.5b04111
Anal. Chem. 2016, 88, 1078−1082

(21) Plouffe, B. D.; Murthy, S. K.; Lewis, L. H. *Rep. Prog. Phys.* **2015**, *78*, 016601.
(22) Deng, H.; Li, X.; Peng, Q.; Wang, X.; Chen, J.; Li, Y. *Angew. Chem., Int. Ed.* **2005**, *44*, 2782−2785.
(23) Ge, J.; Hu, Y.; Biasini, M.; Beyermann, W. P.; Yin, Y. *Angew. Chem., Int. Ed.* **2007**, *46*, 4342−4345.
(24) Liu, J.; Sun, Z.; Deng, Y.; Zou, Y.; Li, C.; Guo, X.; Xiong, L.; Gao, Y.; Li, F.; Zhao, D. *Angew. Chem., Int. Ed.* **2009**, *48*, 5875−5879.
(25) Lee, J. H.; Huh, Y. M.; Jun, Y. W.; Seo, J. W.; Jang, J. T.; Song, H. T.; Kim, S.; Cho, E. J.; Yoon, H. G.; Suh, J. S.; Cheon, J. *Nat. Med.* **2007**, *13*, 95−99.
(26) Jun, Y.-w.; Huh, Y.-M.; Choi, J.-s.; Lee, J.-H.; Song, H.-T.; Kim, S.; Yoon, S.; Kim, K.-S.; Shin, J.-S.; Suh, J.-S.; Cheon, J. *J. Am. Chem. Soc.* **2005**, *127*, 5732−5733.
(27) Dai, D.; Xiang, H.; Whangbo, M. H. *J. Comput. Chem.* **2008**, *29*, 2187−2209.
(28) Knobel, M.; Nunes, W. C.; Winnischofer, H.; Rocha, T. C. R.; Socolovsky, L. M.; Mayorga, C. L.; Zanchet, D. *J. Non-Cryst. Solids* **2007**, *353*, 743−747.

DOI: 10.1021/acs.analchem.5b04111
Anal. Chem. 2016, 88, 1078−1082